Autosegmentation

Automated delineation of brain structures in patients undergoing radiotherapy for primary brain tumors: From atlas to dose–volume histograms

Manuel Conson [a,b], Laura Cella [a,b], Roberto Pacelli [a,b,*], Marco Comerci [b], Raffaele Liuzzi [a,b], Marco Salvatore [a], Mario Quarantelli [a,b]

[a] Department of Advanced Biomedical Sciences, Federico II University School of Medicine; and [b] Institute of Biostructure and Bioimaging, National Research Council (CNR), Naples, Italy

ARTICLE INFO

ABSTRACT

Purpose: To implement and evaluate a magnetic resonance imaging atlas-based automated segmentation (MRI-ABAS) procedure for cortical and sub-cortical grey matter areas definition, suitable for dose-distribution analyses in brain tumor patients undergoing radiotherapy (RT).

Patients and methods: 3T-MRI scans performed before RT in ten brain tumor patients were used. The MRI-ABAS procedure consists of grey matter classification and atlas-based regions of interest definition. The Simultaneous Truth and Performance Level Estimation (STAPLE) algorithm was applied to structures manually delineated by four experts to generate the standard reference. Performance was assessed comparing multiple geometrical metrics (including Dice Similarity Coefficient – DSC). Dosimetric parameters from dose–volume-histograms were also generated and compared.

Results: Compared with manual delineation, MRI-ABAS showed excellent reproducibility [median $DSC_{ABAS} = 1$ (95% CI, 0.97–1.0) vs. $DSC_{MANUAL} = 0.90$ (0.73–0.98)], acceptable accuracy [$DSC_{ABAS} = 0.81$ (0.68–0.94) vs. $DSC_{MANUAL} = 0.90$ (0.76–0.98)], and an overall 90% reduction in delineation time. Dosimetric parameters obtained using MRI-ABAS were comparable with those obtained by manual contouring.

Conclusions: The speed, reproducibility, and robustness of the process make MRI-ABAS a valuable tool for investigating radiation dose–volume effects in non-target brain structures providing additional standardized data without additional time-consuming procedures.

© 2014 Elsevier Ireland Ltd. Radiotherapy and Oncology 112 (2014) 326–331 This is an open access article under the CC BY-NC-SA license (http://creativecommons.org/licenses/by-nc-sa/3.0/).

Late effects, such as cognitive dysfunction (CD), have an important impact on the quality of life [1] of patients bearing brain neoplasms. The correlation between brain irradiation and CD is well recognized. Few data are reported on dose–volume relationships between CD and specific brain substructures [2–4] partly due to the complexity of a reliable delineation of different brain regions for the absence of clear limits among the anatomo-functional areas. The manual brain definition is a time-consuming, prone to error, operator dependent and poorly reproducible process. A magnetic resonance imaging atlas-based automated segmentation (MRI-ABAS) procedure may overcome the drawbacks inherent to manual operation, but the automated process of adapting normal brain atlases may be affected by brain anatomy alterations due to the presence of pathological and/or iatrogenic deformation. Different approaches to segmenting brain with gross abnormalities in an atlas-based framework have been proposed, although in clinical practice their use is still limited [5]. In the radiotherapy (RT) context, MRI-ABAS procedures, taking into account tumor deformation effects, have been suggested and validated by comparing manual and automated delineation of the brain structures. However, these procedures were mainly focused on intracranial structures conventionally considered as organs at risk in brain RT treatment planning, such as brain stem, cerebellum, and optic chiasm [6–8].

The purpose of this work was to validate an MRI-ABAS procedure for cortical and sub-cortical grey matter areas definition, suitable for dose-distribution analyses in studies of RT-related CD. The key elements of the procedure are a preliminary definition of MRI-based grey matter maps and an atlas-based grey matter ROI definition. Our approach is validated by comparing the segmentation results with those obtained through four manual experts' delineations on a dataset of ten patients undergoing 3D conformal radiotherapy for primary brain tumors. The MRI-ABAS procedure performance was assessed by comparing multiple geometrical metrics, along with the dosimetric evaluations obtained by dose–volume-histogram (DVHs) calculations.

* Corresponding author at: Department of Advanced Biomedical Sciences, Università "Federico II", via S. Pansini 5, edificio 10, 80131 Napoli, Italy.
E-mail address: roberto.pacelli@unina.it (R. Pacelli).

Patients and methods

Patients database

We considered ten consecutive patients affected by high grade glioma (who were either biopsied or partially or "completely" resected) treated at our institution. Three-dimensional conformal plans were generated using a commercial treatment planning system (XiO, Elekta CMS). RT was administered using two or more non-coplanar 6 MV photon beams from a linear accelerator with a total dose of 60 Gy in 30 daily fractions of 2 Gy. Before RT, all patients underwent brain MRI (3 Tesla MR scanner Trio, Siemens Medical Systems, Erlangen, Germany). MRI studies included three-dimensional, T1-weighted gradient-echo sequences (MPRAGE, T1 W 1 mm^3 voxel) before and after i.v. injection of contrast medium, diffusion-weighted, FLAIR and TSE-T2 W images in the axial plane. The MPRAGE sequences with contrast medium were used to manually contour the structural parenchyma distortion (deformed area, DA). For each patient, the DA was blindly contoured by four different operators: an expert neuro-radiologist (M.Q.) and three radiation oncologists (M.C., M.S. and R.P.). Treatment details and DA information are reported in Supplementary Table S1.

MRI-ABAS procedure

MRI-ABAS aims at obtaining a set of grey matter regions of interest (ROIs) for each MRI study using a standard atlas of the brain. Accordingly, from the Talairach atlas [9,10] we preliminarily grouped selected brain sub-regions, obtaining the following customized set of 15 brain ROIs: frontal lobes, parietal lobes, occipital lobes, temporal lobes, cingulate gyrus, medial temporal lobes, insular lobes, deep grey matter (i.e. basal ganglia plus thalami) and cerebellum. These ROIs were then superimposed on each patient's MRI using a set of functions included in the Statistical Parametric Mapping software (SPM.8, www.fil.ion.ucl.ac.uk/spm/) as briefly described below.

For each MRI study, a map of the probabilities for each brain voxel belonging to grey matter (GM) was obtained. DAs were used as mask to exclude from the processing the brain voxels with abnormal signal. GM probability map was then converted into a binary map. To transfer the 15 ROIs in the MRI-space an elastic deformation was applied. Finally, the intersection of each ROI in the MRI-space with the GM map provided the automated ROI-set. Further details of the MRI-ABAS procedure are reported in the Supplementary Material Section.

Dosimetric analysis

The ROI-sets were converted in DICOM-RT format using a home-made software (Brain Converter, BRACO) developed in MATLAB (version 7.6.0.324, The Mathworks, Inc., Natick, MA). For each ROI, BRACO extracts the coordinates of the contours and compiles the corresponding RT structure-set file. The MPRAGE sequences without contrast medium were co-registered with the corresponding planning CT-scan using the automated rigid body co-registration method based on the mutual information algorithm embedded in SPM [11]. The RT structure-set files were transferred from the MRI-space into the planning CT-space using the resulting co-registration matrix. Superimposing the dose map from each patient, the dosimetric evaluation was performed using the Computational Environment for Radiotherapy Research (CERR) software [12]. The DVHs were generated for each ROI (automated and manual) and the mean dose (D$_{mean}$), the dose to 95% of volume (D95), and the dose to 5% of volume (D5) were calculated as representative metrics.

The execution time for each study was recorded for both the automated (including DA delineation and computer time) and manual procedures.

Validation procedure

For each study, four sets of manual GM ROIs were generated. To this end, the brain structures were manually delineated on MRI images by the four aforementioned operators, using the Talairach atlas as guidance, and the intersection of each ROI with the GM map provided the manual ROI-set.

The Simultaneous Truth and Performance Level Estimation (STAPLE) algorithm [13] was used to generate, from the four manual ROI-sets, a probabilistic estimate of the reference manual ROI-set (STAPLE-manual), used as ground-truth for the present validation.

Similarly, using the four DA objects defined by each operator, four different automated ROI-sets have been obtained for each study. To assess the influence of the DA contour variability on the automated results, a probabilistic estimate of the reference automated ROI-set (STAPLE-auto) was also obtained.

To quantify inter-operator and between-method differences, the following eight metrics were used: the relative volume differences in ROIs' volumes (ΔVolume, i.e. volume measurement error) and the Dice Similarity Coefficient (DSC, i.e. degree of volumetric overlap) [14] as volumetric measures; the mean absolute surface distance (MSD) [15] and the mean slice-wise Hausdorff distance (MSHD) [15] as shape error measures; the distance between the centres of mass (ΔCOM, i.e. position error) as distance metrics; the differences in D$_{mean}$, D5 and D95 (ΔD$_{mean}$, ΔD5 and ΔD95) as dosimetric measures.

The validation procedure included three evaluations: (a) direct assessment of inter-operator variability and evaluation of MRI-ABAS in this framework, (b) assessment of MRI-ABAS reproducibility with respect to STAPLE-auto, and (c) assessment of MRI-ABAS accuracy with respect to STAPLE-manual.

Inter-operator variability

Pairwise comparisons between each couple of the four operators (identified as R1, R2, R3, R4), and between each operator and STAPLE-auto were performed. This analysis allowed to assess whether STAPLE-auto differed more from the operators than the operators did from each other. Inter-operator analysis was performed by the Mann–Whitney test ($p < 0.05$, two-sided, were considered statistically significant).

Reproducibility

The eight metrics were calculated between automated ROIs and STAPLE-auto (as measure of the robustness of MRI-ABAS in relation to DA contour variability), and compared to the corresponding metrics calculated between manual ROIs and STAPLE-manual. Reproducibility differences between the two methods (MRI-ABAS vs. manual) were assessed by the Wilcoxon's signed-rank test for paired data.

Accuracy

The eight metrics were calculated between automated ROIs and STAPLE-manual. The accuracy of MRI-ABAS was considered as acceptable, when for each metric, the median value fell within the 95% reference interval (e.g. non parametric 95% confidence interval) [16] of the manual method.

All left and right brain structure pairs were combined for both the geometric and the dosimetric analyses.

Results

For the entire ROI-set, the mean execution time for the automated procedure (performed on a hardware platform Intel Core2 Q6600 with 4 GB RAM) compared to manual delineation was 20 vs. 250 min, respectively.

The differences between the automated ROIs and manual ROIs in the MR-space can be essentially appreciated at the interface between adjacent lobes, typically not spanning over more than one sulcus (Fig. 1). Differences in dose–volume distribution between automated RT and manual RT contours are shown in Fig. 2 where an example of DVH comparison for three representative structures of one of the analysed patients is reported.

Inter-operator variability

From the pairwise comparisons analysis, it emerged that the operators significantly differed from each other more than from MRI-ABAS (Supplementary Table S2). Over all structures and all patients, the mean DSC was 0.89 for MRI-ABAS and 0.87 for the operators as group ($p < 0.001$).

Reproducibility

Compared to the manual method, MRI-ABAS showed significantly higher values of DSC, with corresponding lower ΔVolume, MSD, MSHD and ΔCOM values ($p < 0.001$ for all the metrics and regions, Supplementary Table S3). The three dosimetric parameters showed the same behaviour, in agreement with an expected higher reproducibility of the automated procedure (Table 1).

Accuracy

When comparing MRI-ABAS with STAPLE-manual, all the metrics were within the reference interval of the manual method, with the exception of the DSC of insular, frontal, occipital and temporal lobes (Supplementary Table S3). The other metrics out of the reference interval were the MSD of the temporal lobes, and the MSHD of frontal lobes. However, all these ROIs showed overall a median DSC above 0.75 and a MSD lower than 1 mm, suggesting an acceptable degree of accuracy of the automated method compared to manual delineation. The median values of ΔD_{mean}, $\Delta D5$ and $\Delta D95$ for all the automated ROIs were within the reference intervals measured for the manual ROIs (Table 1), thus suggesting a substantial agreement between MRI-ABAS and manual delineation from a dosimetric point of view (Fig. 3).

Discussion

In the present study we implemented a magnetic resonance atlas-based automated segmentation procedure for cortical and sub-cortical grey matter areas definition. The proposed procedure showed to be well-suited for CD-related dose distribution analyses providing additional standardized data without additional time-consuming procedures.

Indeed, to investigate the correlations between irradiation of brain sub-sites and specific side effects, it is essential to identify and outline critical anatomical regions. Moreover, in order to gather and relate clinical variables, a standard and reproducible segmentation methodology should be implemented [1]. In this framework, brain substructures delineation is particularly challenging and the employment of automated delineation procedures could represent a helpful and desirable solution.

In the presence of space occupying lesions and/or deformations, MRI-ABAS procedures have been proposed by several research groups, and the application of the MRI-ABAS procedure to the delineation of conventionally considered OARs in brain RT treatment planning has been investigated [6–8]. Cabezas et al. [5] have reviewed a series of methodologies, characterized by different degrees of complexity, none of which reached the ultimate step of a full dosimetric validation. In addition, commercial ABAS software packages have been recently evaluated [7,17,18]. However, with regard to the cortical and sub-cortical grey matter areas definition, few authors reported on the MRI-ABAS application in the presence of tumor [19–21], and so far no quantitative analysis of the resulting dosimetric accuracy in a clinical setting has been reported.

In this paper we present a robust, reliable and fast MRI-ABAS procedure based on established neuroimaging procedures [22]. All the elements of our framework were integrated in a pipeline that generated the RT structure-set file starting from the CT planning scan, MRI scan and deformed area contour.

The method's performance has been assessed estimating geometric and dosimetric parameters in ten brain tumor patients. After performing the geometric evaluation of MRI-ABAS in the context of inter-operator variability, the automated method has been compared to an estimated ground truth represented by the manual delineations performed by four different operators, optimally merged using STAPLE. From the inter-operator analysis, it emerged that the operators significantly differed from each other more than from MRI-ABAS. In a framework of challenging manual delineation, this evidence suggests the usefulness of an automated method for the brain structures identification.
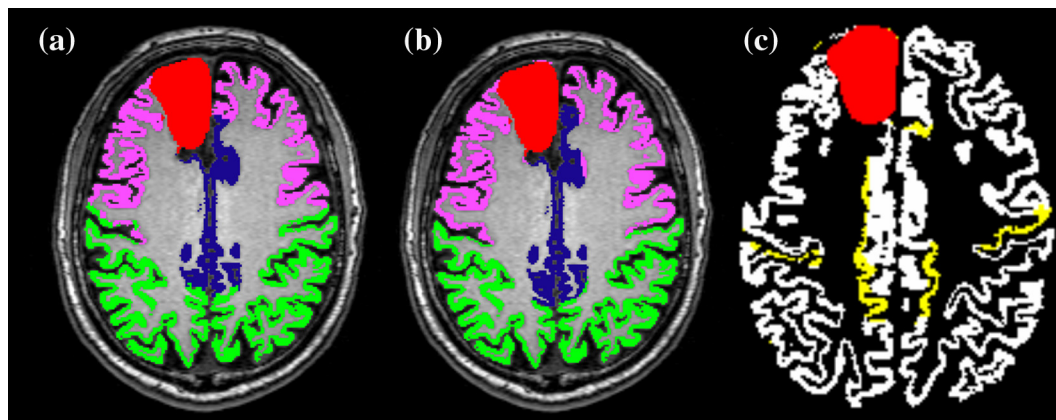

Fig. 1. Automated atlas-based magnetic resonance imaging segmentation (MRI-ABAS) procedure and a single operator manual delineation for one representative patient: (a) atlas-based and (b) manual delineation grey matter ROIs overlay on axial MRI images; (c) overlay on the grey matter map of the subtraction between atlas-based and manual delineation; differences are highlighted in yellow. DA = deformed area (red), FL = frontal lobes (magenta), PL = parietal lobes (green), CG = cingulate gyrus (blue). (For interpretation of the references to color in this figure legend, the reader is referred to the web version of this article.)
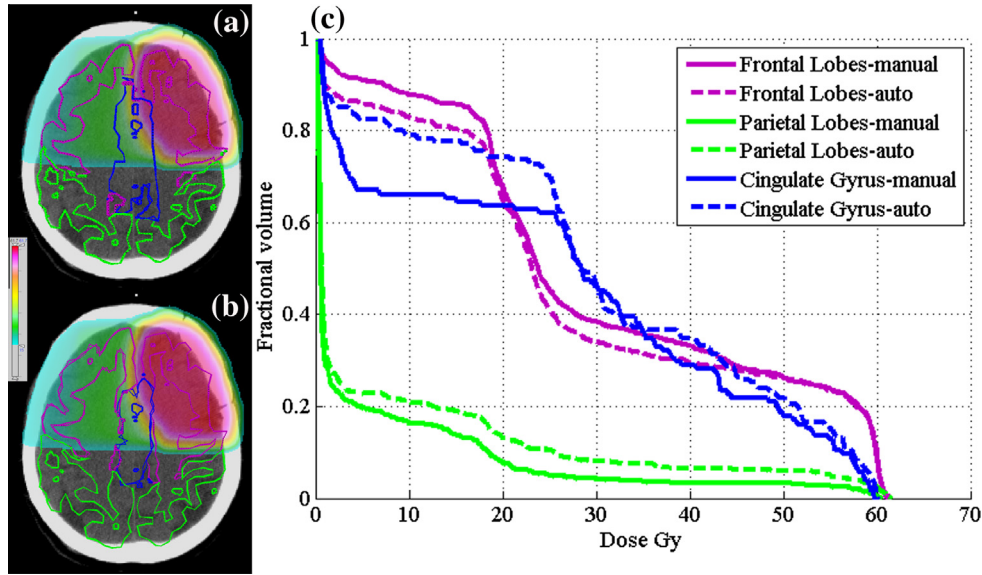
Fig. 2. Dose distributions and dose–volume histograms (DVHs) relative to the automated atlas-based magnetic resonance imaging segmentation (MRI-ABAS) procedure and a single operator manual delineation for one representative patient: (a) the automated RT contours and (b) manual delineation RT contours and the relative dose distribution are overlaid on axial CT images. In (c) the DVHs of cingulate gyrus, frontal and parietal lobes for the automated RT contours (dashed lines) and for the manual delineation contours (solid lines) are reported. Deformed area (red), frontal lobes (magenta), parietal lobes (green), cingulate gyrus (blue). (For interpretation of the references to color in this figure legend, the reader is referred to the web version of this article.)

Table 1
The mean dose (D_{mean}), the dose to 95% of volume (D95) and the dose to 5% of volume (D5) are referred to the ground truth (STAPLE-manual). The median values and the 95% reference intervals for the differences in D_{mean} (ΔD_{mean}), in D95 ($\Delta D95$) and in D5 ($\Delta D5$). All left and right brain structure pairs are combined.

	D_{mean} (Gy)	ΔD_{mean} (Gy)			D95 (Gy)	$\Delta D95$ (Gy)			D5 (Gy)	$\Delta D5$ (Gy)		
		Manual vs. STAPLE manual	Auto vs. STAPLE manual	Auto vs. STAPLE auto		Manual vs. STAPLE manual	Auto vs. STAPLE manual	Auto vs. STAPLE auto		Manual vs. STAPLE manual	Auto vs. STAPLE manual	Auto vs. STAPLE auto
DGM	39.22	0.34 (0.00; 2.07)	0.75 (0.06; 1.49)	0.01 (0.00; 0.19)	16.6	0.36 (0.00; 2.88)	0.44 (0.00; 3.83)	0.02 (0.00; 1.04)	57.59	0.05 (0.00; 1.02)	0.08 (0.01; 0.42)	0.01 (0.00; 0.04)
CBL	16.88	0.15 (0.00; 0.81)	0.16 (0.03; 1.44)	0.00 (0.00; 0.01)	2.95	0.02 (0.02; 0.28)	0.02 (0.00; 0.1)	0.00 (0.00; 0.01)	26.7	0.06 (0.01; 0.96)	0.25 (0.06; 2.73)	0.00 (0.00; 0.04)
CG	36.62	1.71 (0.02; 6.41)	1.78 (0.02; 4.47)	0.01 (0.00; 0.05)	3.71	0.11 (0.00; 13.35)	0.50 (0.02; 2.49)	0.00 (0.00; 0.05)	59.92	0.15 (0.01; 0.63)	0.07 (0.00; 0.47)	0.01 (0.00; 0.06)
FL	28.76	0.53 (0.01; 3.23)	1.22 (0.04; 3.04)	0.01 (0.00; 0.29)	1.19	0.05 (0.00; 3.66)	0.14 (0.00; 16.26)	0.00 (0.00; 0.5)	60.75	0.07 (0.00; 4.97)	0.13 (0.04; 3.49)	0.00 (0.00; 0.06)
INS	27.71	0.36 (0.02; 4.51)	0.66 (0.19; 3.83)	0.01 (0.00; 0.18)	16.82	0.56 (0.00; 8.64)	0.28 (0.02; 9.55)	0.01 (0.00; 0.40)	56.02	0.10 (0.00; 1.38)	0.15 (0.02; 1.72)	0.00 (0.00; 0.22)
MTL	26.5	0.56 (0.00; 3.92)	0.47 (0.03; 3.69)	0.01 (0.00; 0.35)	16.78	0.27 (0.01; 3.05)	0.35 (0.00; 16.28)	0.00 (0.00; 0.08)	45.77	0.36 (0.00; 6.35)	0.98 (0.02; 15.72)	0.01 (0.00; 1.64)
OL	16.93	0.39 (0.01; 2.77)	0.53 (0.01; 2.67)	0.00 (0.00; 0.04)	10.64	0.14 (0.01; 6.15)	0.16 (0.00; 5.74)	0.00 (0.00; 0.06)	25.67	0.30 (0.00; 5.65)	0.22 (0.01; 3.06)	0.01 (0.00; 0.06)
PL	23.89	0.78 (0.02; 5.37)	0.59 (0.01; 2.14)	0.01 (0.00; 0.11)	4.28	0.19 (0.00; 33.96)	0.17 (0.00; 12.91)	0.00 (0.00; 0.20)	56.63	0.55 (0.00; 17.13)	0.26 (0.00; 12.47)	0.01 (0.00; 0.42)
TL	22.95	0.71 (0.02; 6.04)	1.07 (0.12; 5.40)	0.00 (0.00; 0.05)	1.61	0.14 (0.01; 1.77)	0.12 (0.00; 2.08)	0.00 (0.00; 0.09)	48.24	0.44 (0.05; 4.60)	0.79 (0.02; 6.16)	0.00 (0.00; 0.17)
Overall		0.52 (0.01; 4.21)	0.65 (0.02; 3.83)	0.01 (0.00; 0.14)		0.13 (0.00; 7.71)	0.16 (0.00; 12.90)	0.00 (0.00; 0.23)		0.17 (0.00; 6.73)	0.23 (0.01; 9.10)	0.01 (0.00; 0.24)

Abbreviations: Frontal lobes (FL), parietal lobes (PL), occipital lobes (OL), temporal lobes (TL), cingulate gyrus (CG), medial temporal lobes (MTL), insular lobes (INS), deep grey matter (DGM) and cerebellum (CBL).

An expected result is represented by the higher reproducibility of the automated method when compared with the manual delineation procedure in terms of spatial overlap, surface error and posi-tion error. Due to the relative insensitivity of MRI-ABAS to the variations of the deformed area, the high degree of reproducibility suggests that the proposed method is robust. The significantly
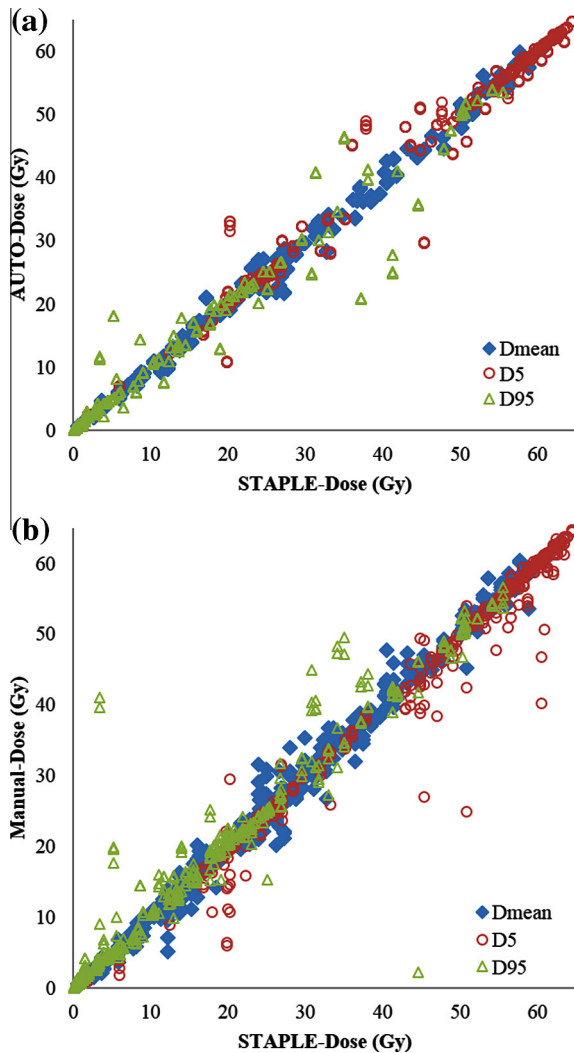
Fig. 3. Correlation plots relative to the dosimetric parameters from (a) the automated RT contours and from (b) the manual RT contours from all individual operators with respect to STAPLE-manual. The mean dose (D_{mean}, blue diamond), the dose to 5% of volume (D5, red circle), and the dose to 95% of volume (D95, green triangle) are reported. The correlation plots illustrate the overall agreement with respect to the ground truth (STAPLE-manual) for both MRI-ABAS and manual delineation. (For interpretation of the references to colour in this figure legend, the reader is referred to the web version of this article.)

higher reproducibility of MRI-ABAS resulted also in a higher reproducibility in terms of dosimetric parameters.

As to accuracy, the spatial overlap was overall satisfactory: the median DSC being 0.81 (95% CI, 0.68–0.94). The values of spatial overlap are comparable to those reported by other authors for similar, although not identical, brain structures. Isambert et al. [7] concluded that automated segmentation was well suited for organs like cerebellum, with DSC values around 0.8–0.9, while smaller structures showed lower values (0.4–0.5). In our case also, the highest DSC values were observed for larger structures like the cerebellum and frontal lobes (0.94 and 0.87, respectively), while the lowest DSC values were obtained for medial temporal lobes (0.78), for insular lobes and the cingulated gyrus (0.75). Of course, other factors, such as the shape of the structures and their position within the brain, can also have an effect in this respect [8].

Of note, the DSC median values for all the structures that fell outside the reference intervals were nonetheless above 0.7. This threshold is generally considered as indicative of an acceptable overlap in the validation studies of biomedical image processing techniques [23,24], although further evidence will be needed in

the future to support this cut-off value in the context of RT-related CD studies. Interestingly, for frontal and temporal lobes the MRI-ABAS showed an accuracy below the reference intervals defined by the manual method despite median DSC values above 0.80 in both cases. This is due to the high reproducibility of the manual delineation of these structures which have large sizes and relatively clear anatomical boundaries. The shape and position errors for MRI-ABAS were comparable with those derived from the manual delineation.

Of note, in defining the acceptability criteria for the accuracy of the automated method, our aim was to compare the accuracy of the latter to an estimate of the range of possible segmentations obtained manually (defined for each structure by a reference interval), rather than to demonstrate that the automated method was at least as accurate as the manual one (which had an obvious advantage due to the use of STAPLE-manual as ground truth).

Considering the impact of the automated procedure on dosimetric endpoints, the MRI-ABAS procedure provides results comparable to those obtained by manual delineation: the distributions of the median ΔD_{mean}, $\Delta D5$ and $\Delta D95$ for the automated contours were similar to the corresponding dosimetric parameters obtained by the manual contours (Fig. 3). Although the dosimetric accuracy measures of MRI-ABAS were always within the reference intervals, and despite the fact that the median values never exceeded 1 Gy, it must be pointed out that for some structures (medial temporal and parietal lobes) the differences with the ground truth could exceed 10 Gy. However, for the parietal lobe the $\Delta D95$ reference interval exceeded 10 Gy also with the manual method. This is likely due to the difficulty for the manual operator to recognize boundaries that, at least in part for the parietal lobe, are barely discernible. On the other hand, for the medial temporal lobe, the above mentioned limitations, associated to the relatively small size of the structure, may in some cases result in larger errors requiring the manual editing of this structure.

In general, it should be pointed out that the results of the present validation cannot be extrapolated to other brain structure subdivisions, even if of similar shape and size. Similarly, our analyses were performed in a 3D-conformal RT setting and the dosimetric results may be different when different radiation techniques are used.

In conclusion, the proposed framework for automated delineation of brain regions in a radiotherapy context was found to be feasible and efficient. The proposed framework shows substantial efficiency with at least 90% reduction in delineation time while maintaining comparable accuracy and improving reproducibility from both a geometric and dosimetric point of view. The execution time may be further reduced using higher performance machines when large samples have to be handled. Our pipeline has been conceived to be integrated in the clinical radiotherapy process that leads to the construction of treatment planning. All this makes MRI-ABAS a valuable tool for investigating radiation dose–volume effects in non-target brain structures.

Conflict of interest

All authors of this paper declare no competing financial interest.

Acknowledgment

The authors thank Dr. Maria Pia Graziani for useful suggestions.

Appendix A. Supplementary data

Supplementary data associated with this article can be found, in the online version, at http://dx.doi.org/10.1016/j.radonc.2014.06.006.

References

[1] Lawrence YR, Li XA, el Naqa I, et al. Radiation dose–volume effects in the brain. Int J Radiat Oncol Biol Phys 2010;76:S20–27.

[2] Hsiao KY, Yeh SA, Chang CC, et al. Cognitive function before and after intensity-modulated radiation therapy in patients with nasopharyngeal carcinoma: a prospective study. Int J Radiat Oncol Biol Phys 2010;77:722–6.

[3] Jalali R, Mallick I, Dutta D, et al. Factors influencing neurocognitive outcomes in young patients with benign and low-grade brain tumors treated with stereotactic conformal radiotherapy. Int J Radiat Oncol Biol Phys 2005;77:974–9.

[4] Gondi V, Hermann BP, Mehta MP, et al. Hippocampal dosimetry predicts neurocognitive function impairment after fractionated stereotactic radiotherapy for benign or low-grade adult brain tumors. Int J Radiat Oncol Biol Phys 2012;83:e487–493.

[5] Cabezas M, Oliver A, Llado X, et al. A review of atlas-based segmentation for magnetic resonance brain images. Comput Methods Programs Biomed 2011;104:e158–177.

[6] Bondiau PY, Malandain G, Chanalet S, et al. Atlas-based automatic segmentation of MR images: validation study on the brainstem in radiotherapy context. Int J Radiat Oncol Biol Phys 2005;61:289–98.

[7] Isambert A, Dhermain F, Bidault F, et al. Evaluation of an atlas-based automatic segmentation software for the delineation of brain organs at risk in a radiation therapy clinical context. Radiother Oncol 2008;87:93–9.

[8] Deeley MA, Chen A, Datteri R, et al. Comparison of manual and automatic segmentation methods for brain structures in the presence of space-occupying lesions: a multi-expert study. Phys Med Biol 2011;56:4557–77.

[9] Lancaster JL, Rainey LH, Summerlin JL, et al. Automated labeling of the human brain: a preliminary report on the development and evaluation of a forward-transform method. Hum Brain Mapp 1997;5:238–42.

[10] Lancaster JL, Woldorff MG, Parsons LM, et al. Automated Talairach atlas labels for functional brain mapping. Hum Brain Mapp 2000;10:120–31.

[11] Collignon A, Maes, F., Delaere, D., Vandermeulen, D., Suetens, P., Marchal, G. Automated multimodality image registration based on information theory. In: International conference on information processing in medical imaging – IPMI'95, vol. 3. Kuwer Academic Publishers; 1995. p. 263–74.

[12] Deasy JO, Blanco AI, Clark VH. CERR: a computational environment for radiotherapy research. Med Phys 2003;30:979–85.

[13] Warfield SK, Zou KH, Wells WM. Simultaneous truth and performance level estimation (STAPLE): an algorithm for the validation of image segmentation. IEEE Trans Med Imaging 2004;23:903–21.

[14] Dice LR. Measures of the amount of ecologic association between species. Ecology 1945;26:297–302.

[15] Gerig G, Jormier M, Chakos M. A new validation tool for assessing and improving 3D object segmentation. MICCAI 2001: 516–23.

[16] Horowitz G. Establishing, and verifying reference intervals in the clinical laboratory; approved guideline. 3rd ed. C28A3E: Clinical and Laboratory Standards Institute; 2008.

[17] Stapleford LJ, Lawson JD, Perkins C, et al. Evaluation of automatic atlas-based lymph node segmentation for head-and-neck cancer. Int J Radiat Oncol Biol Phys 2010;77:959–66.

[18] La Macchia M, Fellin F, Amichetti M, et al. Systematic evaluation of three different commercial software solutions for automatic segmentation for adaptive therapy in head-and-neck, prostate and pleural cancer. Radiat Oncol 2012;7:160.

[19] Pollo C, Cuadra MB, Cuisenaire O, et al. Segmentation of brain structures in presence of a space-occupying lesion. NeuroImage 2005;24:990–6.

[20] Popple RA, Griffith HR, Sawrie SM, et al. Implementation of Talairach atlas based automated brain segmentation for radiation therapy dosimetry. Technol Cancer Res Treat 2006;5:15–21.

[21] Stefanescu R, Commowick O, Malandain G, et al. Non-rigid atlas to subject registration with pathologies for conformal brain radiotherapy. In: Int. conf. med. image comput. comput. assist. interv, Saint Malo, France; 2004. p. 704–11.

[22] Brett M, Leff AP, Rorden C, et al. Spatial normalization of brain images with focal lesions using cost function masking. NeuroImage 2001;14:486–500.

[23] Zijdenbos AP, Dawant BM, Margolin RA, et al. Morphometric analysis of white matter lesions in MR images: method and validation. IEEE Trans Med Imaging 1994;13:716–24.

[24] Anders LC, Stieler F, Siebenlist K, et al. Performance of an atlas-based autosegmentation software for delineation of target volumes for radiotherapy of breast and anorectal cancer. Radiother Oncol 2012;102:68–73.